

Suspended Microchannel Resonators for Ultralow Volume Universal Detection

By

Sungmin Son

B.S., School of Mechanical and Aerospace Engineering
Seoul National University, 2006

Submitted to the Department of Mechanical Engineering
In Partial Fulfillment of the Requirements for the Degree of
Master of Science in Mechanical Engineering

at the

Massachusetts Institute of Technology

[June 2008]
August 2008

© 2008 Massachusetts Institute of Technology
All rights reserved

Signature of Author.....

Department of Mechanical Engineering
May 12, 2008

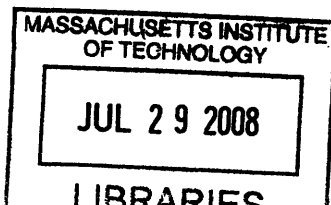
Certified by.....

Scott Manalis
Professor of Mechanical and Biological Engineering
Thesis Supervisor

Accepted by.....

Lallit Anand

Chairman, Department Committee on Graduate Students



ARCHIVES

Suspended Microchannel Resonators for Ultralow Volume Universal Detection

By

Sungmin Son

Submitted to the Department of Mechanical Engineering
On May 12, 2008 in Partial Fulfillment of the
Requirements for the Degree of Master of Science in
Mechanical Engineering

ABSTRACT

Universal detectors that maintain high sensitivity as the detection volume is reduced to the sub-nanoliter scale can enhance the utility of miniaturized total analysis systems (μ -TAS). Here the unique scaling properties of the suspended microchannel resonator (SMR) are exploited to show universal detection in a 10 pL analysis volume with a density detection limit of $\sim 1 \mu\text{g}/\text{cm}^3$ (10 Hz bandwidth) and a linear dynamic range of six decades. Analytes with low UV extinction coefficients such as polyethylene glycol (PEG) 8 KDa, glucose, and glycine are measured with molar detection limits of 0.66 μM , 13.5 μM , and 31.6 μM , respectively. To demonstrate the potential for real-time monitoring, gel filtration chromatography was used to separate different molecular weights of PEG as the SMR acquired a chromatogram by measuring the eluate density. This work suggests that the SMR could offer a simple and sensitive universal detector for various separation systems from liquid chromatography to capillary electrophoresis. Moreover, since the SMR is itself a microfluidic channel, it can be directly integrated into μ -TAS without compromising overall performance.

Thesis Supervisor: Scott Manalis

Title: Professor of Mechanical and Biological Engineering

Acknowledgements

First of all, I wish to thank Professor Scott Manalis for the opportunity to do my thesis research in his laboratory. Scott has given me invaluable guidance that fosters creativity, teamwork, enthusiasm, and hands-on research. I also want to thank all group members who contributed to this work: Thomas Burg originally developed the SMR and related setups which I used for my research inline with HPLC system. He also gave me countless advices regarding experiment. Will Grover was an indispensable resource for everything from the knowledge involving HPLC to experimental details. Michel Godin was a good consultant who gave me an insight to research in general. Scott Knudsen helped me dealing with problems involving chemistry and biology with great passion. Yao-Chung (Wesley) Weng gave me a great help in dealing with electronics such as oscillating circuits. Furthermore, the passion of Rumi Chunara, diligence of Andrea Bryan, optimism of Marcio von Muhlen, and discretion of Phillip Dextras has been constant sources of motivation for me. I also thank Ken Babcock and Alison Skelley for valuable discussions.

Finally, I am deeply grateful to my parents and my brother for their love and support in my academic journey.

Funding for this research was provided by the National Institutes of Health (NIH) Grant EB003403, the National Institute of General Medical Sciences (NIGMS) Cell Decision Process Center Grant P50-GM68762 and Korean Electric Power Research Institute (KEPRI).

Contents

1. Introduction	7
1.1 Background and motivation	7
1.1.1 Universal detection in HPLC.....	7
1.1.2 Microscale separation.....	7
1.2 Objectives.....	8
2. Theories, methods, and materials	9
2.1 HPLC detectors	9
2.2 Suspended microchannel resonator	10
3. Experiment	13
3.1 Chemicals.....	13
3.2 Experimental setup.....	13
3.3 Detection scheme	15
4. Results and discussion	16
4.1 Limit of detection.....	16
4.2 Dynamic range	18
4.3 Chromatogram.....	20
4.4 Gradient elution.....	21
4.5 Peak dispersion.....	25
5. Conclusion	28
6. Appendix	29
7. References	30

LIST OF FIGURES

1. Illustration of two mass measurement modes of the SMR.....	16
2. Flow diagram of the SMR.....	16
3. Frequency-concentration curve of the SMR to various concentrations of PEG 8KDa.....	16
4. Peak response of the SMR to the mobile phase as input.....	16
5. Frequency response of the SMR to air and water.....	16
6. Chromatograms of the SMR and the UV detector resulting from a five-component mixture of PEG.....	20
7. Chromatograms resulting from the two serial runs of the identical gradient elution with or without the sample injection.....	22
8. Compensated chromatogram of the UV detector resulting from the elimination of the baseline signal.....	23
9. Compensated chromatogram of the SMR resulting from the elimination of the baseline signal.....	24
10. Graphical representation of the diffusion and the convection of the peak inside the detection cell.....	26
11. Simulated response of the SMR and the UV detector for a small sample injection.....	27

LIST OF TABLES

1. Limit of detection of SMR for various analytes.....	17
2. Typical properties of the SMR and common HPLC detectors.....	18

Introduction

1.1 Background and motivation

1.1.1 Universal detection in HPLC

Among the various detection methods for high performance liquid chromatography (HPLC) [1], universal detectors provide an important alternative to the commonly used UV – Visible detectors as they can analyze chemicals without chromophores or fluorophores [2]. For example, evaporative light scattering detectors (ELSD) have been used to detect nonvolatile compounds such as lipids [3], carbohydrates [4], and pharmaceutical compounds [5, 6], which exhibit weak optical absorbance in the UV-Visible region. However, ELSD is considered a semi-universal detector because the sensitivity depends strongly on the volatility of the analytes and mobile phases [7]. The refractive index detector (RID), which is the most widely used universal detector [8], responds to essentially all analytes without requiring modification of the sample [9]. State-of-the-art commercial RID achieve detection limits on the order of 10^{-9} refractive index units (RIU) for volumes on the microliter scale [10]. For samples where the signal-to-noise of the differential mass density is greater than the differential refractive index [11], densitometry can be used in place of RID to improve sensitivity. For example, Trathnigg *et al.* used an oscillating glass capillary tube to measure density with a detection limit of $0.35 \mu\text{g}/\text{cm}^3$ in a volume of $20 \mu\text{L}$. For glycine, such a detection limit is roughly equivalent to 2×10^{-11} RIU, which is nearly 100-fold more sensitive than the commercial RID.

1.1.2 Microscale separation

Proliferation of miniaturized analysis techniques such as micro high performance liquid chromatography (μHPLC) and capillary electrophoresis (CE) has led to the necessity of on-column [12] analysis of solutes in nanoliter to picoliter volumes with high sensitivity and in the absence of derivatization chemistry [13, 14]. As UV absorption does not scale favorably due to path length dependency [12, 15] and nonlinear response to sample concentration [16], effort is being directed towards maintaining high sensitivity with RID while scaling the detection volume down to the nanoliter regime. For example, Wang *et al.* developed dual-capillary dual-bicell micro interferometric backscattering detection [17] that achieved a sensitivity of 10^{-9} RIU in a 50 nL detection volume. As an extension of this work, Bornhop *et al.* achieved a detection limit of 10^{-6} RIU in a 350 pL volume with a simple and elegant approach that required only a helium-neon laser, a microfluidic channel, and a position sensor [18]. Effort is also being directed towards

developing miniaturized densitometers. Corman *et al.* demonstrated a detection limit of $4 \mu\text{g}/\text{cm}^3$ in a $35 \mu\text{L}$ volume with a low-pressure encapsulated silicon densitometer with integrated feedback control electronics [19], and Sparks *et al.* used a related approach to achieve a detection limit of $28 \text{g}/\text{cm}^3$ in a $0.6 \mu\text{L}$ volume [20]. These results, in light of those by Trathnigg *et al.*, indicate that densitometers can maintain high sensitivity as the analysis volume is reduced.

1.2 Objectives

In this paper, we show that the suspended microchannel resonator (SMR) can be used as a universal detector to resolve relative density changes of $1 \mu\text{g}/\text{cm}^3$ within a volume of 10pL . The SMR differs from the aforementioned densitometers both in terms of scale and sensitivity: the combination of the low resonator mass (100ng) and high quality factor ($15,000$) enables a minimum detectable mass of approximately one femtogram [21]. To demonstrate the utility of the SMR for real-time detection, we have coupled it to HPLC and measured the response from various analytes introduced by liquid mobile phases. We discuss the analytical attributes of linearity, dynamic range, sensitivity, and noise considerations, and we present a comparison between the HPLC-SMR and conventional HPLC-UV-Visible. Since the SMR is manufactured by conventional semiconductor fabrication processes, it can ultimately be integrated with upstream microfluidic sample preparation and separation stages to create a miniaturized total analysis system.

1. Theories, methods, and materials

2.1 HPLC detectors

Ever since the inception of Liquid Chromatography (LC), the performance of the detector has taken an important role in the LC since the improvement of the detector has enabled access to the new columns with reduced dispersion and higher efficiencies. This improvement was mainly attributed to the minimum dispersion, wide dynamic range, linear response, low noise and high sensitivity of current LC detectors. The LC detectors range from those that are exclusively non specific (e.g., the refractive index detector) through those that are partially specific (e.g., the UV detectors) to the totally specific detectors (e.g., the fluorescence detector). In general, the sensitivity increases progressively as the detector becomes more specific, the highest sensitivities being obtained from the specific detectors [22].

The UV detector is by far the most popular and useful LC detector. Although the UV detector has some definite limitations (particularly for the detection of non-polar solutes that do not possess UV chromophores) it has the best combination of sensitivity, linearity, and reliability of all the LC detectors so far developed [23]. There are two factors that control the detector sensitivity: the magnitude of the extinction coefficient of the solute being detected and the path length of the light passing through the cell. The magnitude of the extinction coefficient depends on the wavelength of the UV light resulting in the specificity of the UV detector. The path length of the UV detector affects not only the sensitivity but also the dispersion of peaks inside the detector cell. Hence, while the path length should be long enough to maintain the high sensitivity, it cannot be increased indefinitely because long cells will provide excessive peak dispersion with consequent loss of column resolution. Furthermore, as the separation columns generate peaks of smaller volume in modern chromatography, the detector cell is required to have smaller volume as well.

The refractive index (RI) detector is considered not sensitive compared to other LC detectors since it responds to changes in ambient temperature, pressure changes, and flow rate changes and cannot be used in gradient elution. However, unlike ELSD, the RI detection features a number of advantages in comparison to UV or fluorescence detection. First, it is noninvasive to virtually all analytes. Second, it is relatively simple to implement and provides a sensing signal regardless of whether absorbing or fluorescent chromophores are present in the sample. Due to these properties, the RI detector has the unique area of application in the separation and analysis of polymers or carbohydrates since they do not adsorb in the UV, do not ionize and although fluorescent derivatives can be made, the procedure is tedious and time consuming. Moreover, since the RI detector measures the analyte concentration instead of mass, the detection signal does not scale down

with the sample volume, which makes RI detection particularly attractive when ultrasmall (pico-/nanoliter) detection volume is involved [24].

The evaporate light scattering detector (ELSD) can offer distinct advantages over the UV and RI detector for particular applications due the unique mechanism. In LC combined with ELSD, the eluate from a chromatographic column is converted to an aerosol by a nebulizer with the aid of carrier gas. The aerosol is then carried into a heated drift tube where the solvent is evaporated to form small analyte particles that can arouse the light scattering. Since the scattered light is proportional to the amount of sample and is not dependent on a specific functional group or on chromophores, the technique is a powerful tool for detecting any sample that is less volatile than the mobile phase, irrespective of the optical properties of the compounds of interest. The ELSD is suitable to detect nonvolatile compounds such as lipids, carbohydrates, and pharmaceutical compounds, which show weak optical absorbance in the UV-Visible region. However, the ELSD is unable to be applied to the measurement of volatile analytes [25].

2.2 Suspended microchannel resonator

Suspended microchannel resonator (SMR), the nanomechanical resonator that enables the measurement of mass with extraordinary sensitivity, has been previously developed in our group [21]. Elimination of viscous damping by placing the sample solution inside a hollow resonator that is surrounded by vacuum gives the SMR a high quality factor, which in turn gives high sensitivity. In particular, dry resonators possess quality factors up to 15,000 and exhibit a frequency stability of 10 p.p.b. (parts per billion) in a 1 Hz bandwidth, even when the suspended microchannel is subjected to continuous flow. Among the various intriguing applications, such as mass-based flow cytometry, the direct detection of pathogens, or the non-optical sizing and mass density measurement of colloidal particles, the measurement of bulk fluid density is one of the most basic and important applications.

As shown in figure 1, changes in mass inside the channel translate into shifts in the resonance frequency, f , according to:

$$f = \frac{1}{2\pi} \sqrt{\frac{k}{m^* + 0.24\Delta m}} \quad (1)$$

(k : spring constant, m^* : effective mass, Δm : added mass)

Since the added mass is derived from the bulk density change of the eluate, Δm is equal to $\Delta\rho V$, where $\Delta\rho$ is the density change of the eluate and V is the volume of the resonator. Hence, the more the density of the

eluate differs from that of the mobile phase, the higher the response. This detection mechanism makes the SMR universal and especially beneficial for size exclusion chromatography, where the sample is much heavier than the mobile phase and usually only one mobile phase is enough for one entire elution. For example, one of the main beneficiaries of the SMR detection scheme will be the polymer industry, where size exclusion chromatography is widely used to characterize the polymer. Particularly, finer characterization of polymers can directly contribute to the polymer solar cell development, in which better characterization of light emitting polymers is crucial.

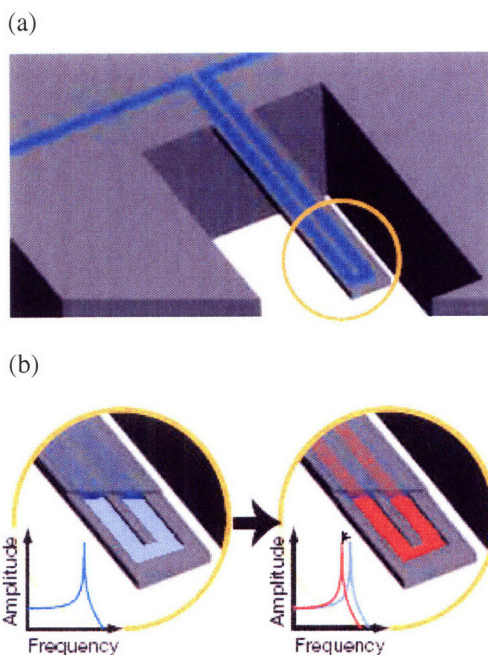


Figure 1. Illustration of two mass measurement modes enabled by a fluid-filled microcantilever. (a) A suspended microchannel translates mass changes into changes in resonance frequency. Fluid continuously flows through the channel and delivers eluate. (b) As the channel contents are replaced from pure mobile phase to eluate, the mass of microcantilever changes, resulting in the shift of the resonant frequency.

The SMR has favorable scaling properties, which facilitate its integration into micro total analysis systems (μ TAS) without compromising overall performance. After Taylor expansion of the frequency-mass relationship of the SMR to first order, the sensitivity is estimated as

$$\frac{\Delta w}{\Delta m} \approx -\frac{w_0}{2m} = -\frac{\sqrt{k}}{2m^{3/2}} \quad (2)$$

(k: spring constant, m: the mass of the resonator)

Since Δm is equal to $\Delta \rho V$ and $\Delta \rho$ is proportional to the change of sample concentration, the lighter the resonator is, the more the frequency changes upon the same sample concentration change given the V is constant. However, in practice the volume of the resonator V decreases as the resonator gets smaller, and the overall sensitivity relies on the relationship:

$$\frac{\Delta w}{\Delta \rho} \approx -\frac{V\sqrt{k}}{2m^{3/2}} \quad (3)$$

Therefore, the size of the SMR can be reduced for integration into μ -TAS without compromising the overall sensitivity given that the volume of the cavity inside the resonator and the mass of the resonator are properly designed. On the other hand, the UV detector cannot be similarly minimized because of the path length dependency. UV absorbance is expressed as $A = \epsilon c l$ (ϵ : molar extinction coefficient, l: path length, c: concentration), which means the sensitivity is equal to $\frac{\Delta A}{\Delta c} = \epsilon l$. Therefore, the shorter the path length is, the less the absorbance changes upon the same sample concentration change.

3. Experiment

3.1 Chemicals

Polyethylene glycol (PEG) 4kDa, 8 kDa and 20 kDa were purchased from Sigma Chemical Co. (St. Louis, MO), 1 kDa and 31 kDa from Polymer Laboratories (Shropshire, UK). L-glucose, glycine and bovine serum albumin (BSA) were obtained from Sigma Chemical Co. (St. Louis, MO). Acetonitrile and toluene were purchased from Sigma Chemical Co. (St. Louis, MO). All solutions were prepared with water purified by a Millipore Simplicity system (Millipore, Bedford, MA).

3.2 Experimental setup

A description of the SMR device and its operation may be found in chapter 2.2. For the device used in this work, the density sensitivity of $10470 \text{ Hz}/(\text{g cm}^{-3})$ was measured by using solvents of known density such as water, acetonitrile and toluene.

The HPLC system consisted of an Agilent 1100 HPLC system (Agilent Technologies, Palo Alto, CA, USA) including a binary LC pump, micro autosampler with a six-port switching valve equipped with a loop volume of $40 \mu\text{L}$, and a multi-wavelength detector (MWD) with an 80 nL , 6 mm path length flow cell. Micro flow mode with a $100 \mu\text{L}/\text{min}$ maximum was used to precisely adjust the flow rate of the mobile phase for the flow injection analysis and gel filtration chromatography (GFC). Sample injection and flow adjustment were entirely automated. For gel filtration chromatography, Tosoh Bioscience SuperSW3000 gel filtration column (30 cm length, 2 mm i.d., $4 \mu\text{m}$ particle size, $500,000 \text{ Da}$ pore size) was used without a guard column. For reverse phase chromatography, Zorbax SB C18 reverse phase column was used without a guard column.

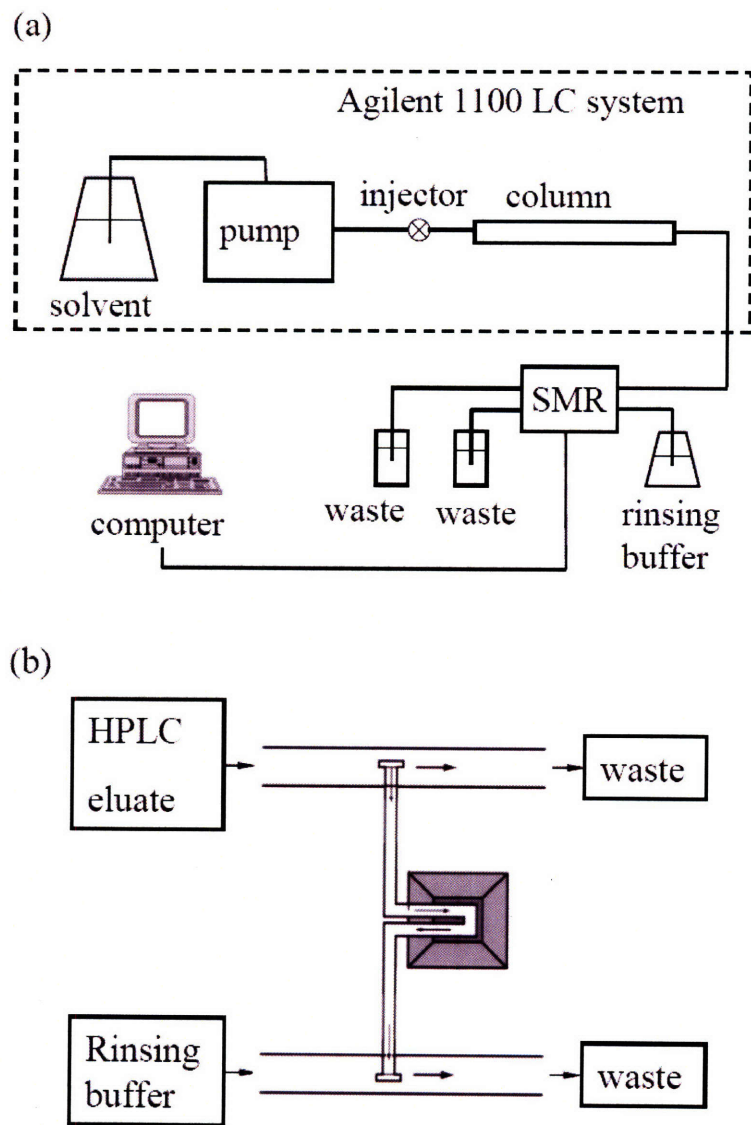


Figure 2. (a) Flow diagram of the suspended microchannel resonator (SMR) detection system. Solution leaving the column enters a small-volume (10 pL) suspended microchannel (b) which reports on the density of the eluate. The density monitored as a function of separation time produces a chromatogram. Since the flow cross-section of suspended microchannel is about 70 times smaller than that of the bypass channels, only $\sim 1/3000$ of the bypass flow is directed into the suspended microchannel. The linear flow rate through the suspended microchannel is ~ 13 mm/sec when the volumetric flow rate through the column is $65 \mu\text{L}/\text{min}$.

Figure 2 (a) shows a schematic diagram of the HPLC-SMR apparatus. A 5 cm length of PEEK tubing (1/32 in. o.d. \times 0.010 in. i.d.) was used to connect the injector valve to the separation column. The eluate was sent to either the SMR or the MWD. A 12 cm length of PEEK tubing (1/32 in. o.d. \times 0.0025 in. i.d.) was used to connect the column to the MWD. A 20 cm length of FEP tubing (1/32 in. o.d. \times 0.003 in. i.d.) was used to connect the column to the SMR. For flow injection analysis, a 30 cm length of PEEK tubing (1/32 in. o.d. \times 0.010 in. i.d.) was used along with a micro-tight union (Upchurch Scientific) to connect the injector valve to either the SMR or MWD instead of the column.

Figure 2 (b) shows the flow path in the bypass channels and the suspended microchannel of the device. Two 10 nL bypass channels were needed to decrease the flow resistance and accommodate the flow rate of 65 μ L/min, which is optimal for GFC. While most of the HPLC eluate flows out to the waste reservoir of the upper bypass channel, a small portion flows through the suspended microchannel. The flow rate through the suspended microchannel is determined by the pressure difference between its inlet and outlet. Since the flow cross-section of the suspended microchannel is about 70 times smaller than that of the bypass channels, the linear flow rate can be much faster in the suspended microchannel than in the bypass channel, even though the pressure difference across the suspended microchannel is small. Therefore, at any given time, it is assumed that the SMR is measuring the eluate that is present at the inlet of the suspended microchannel. For a flow rate of 65 μ L/min in one bypass channel and a pressure of \sim 6 psi in the inlet of the other bypass channel regulated using precision pressure regulators (Omega Engineering, PRG101-25), the pressure difference across the suspended microchannel was \sim 10 psi, leading to the linear flow rate of 13 mm/sec through the suspended microchannel.

3.3 Detection scheme

The \sim 200 kHz mechanical resonant frequency of the SMR is mixed down with a reference oscillator whose frequency is \sim 1 kHz below the resonant frequency. The down-converted signal is then rectified and measured with the time-frequency counter (National Instruments PCI-MIO-16 multifunctional DAQ card). With this scheme, the data acquisition rate is dictated by the frequency of the mixed-down signal (\sim 1 kHz). Noise is reduced off-line using a Savitzky-Golay filter and a moving average filter, resulting in a final sampling rate of 10 Hz.

4. Results and discussion

4.1 Limit of detection

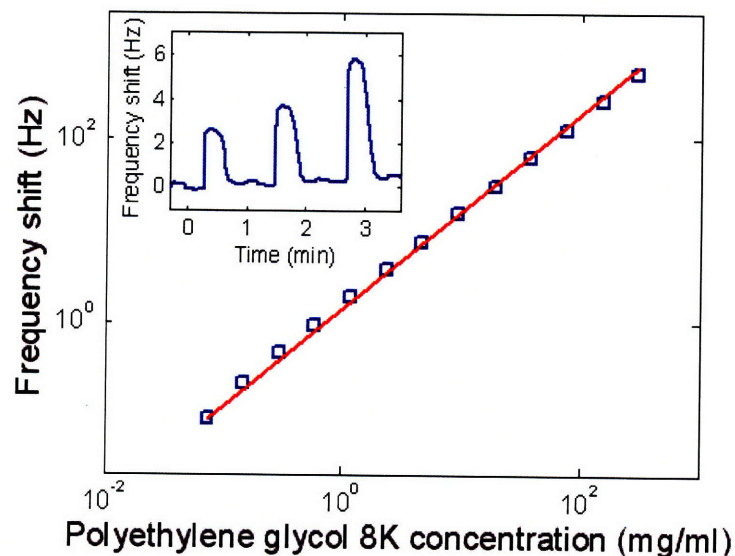


Figure 3. Various concentrations of PEG 8kDa were measured from the most dilute to the most concentrated with a 15 $\mu\text{L}/\text{min}$ flow rate and without the column. Inset shows the SMR time response to three different concentrations of PEG (0.59 mg/ml, 1.2 mg/ml, and 2.3 mg/ml each). The relative height of the peak from the baseline was used to determine each point of the frequency-concentration curve.

The linearity of the SMR was determined by injecting 30 μL sample plugs of 8 kDa PEG without a column at concentrations ranging from 0.1 mg/ml to its maximum solubility of ~ 300 mg/ml (Figure 3). The inset of figure 3 shows the SMR frequency response to the saturated peak versus time for 3 different concentrations of PEG. Baseline instability between peaks was primarily due to pressure variations across the SMR created by the sample exchange valve. As a control, only the mobile phase (water) was injected following each PEG sample, and as shown in figure 4 a reproducible peak response that was independent of the sample concentration was routinely observed. This offset was attributed to nonspecific contamination entering the SMR from the HPLC fluid path. To accommodate for this offset, the response from the mobile phase was subtracted from each sample response.

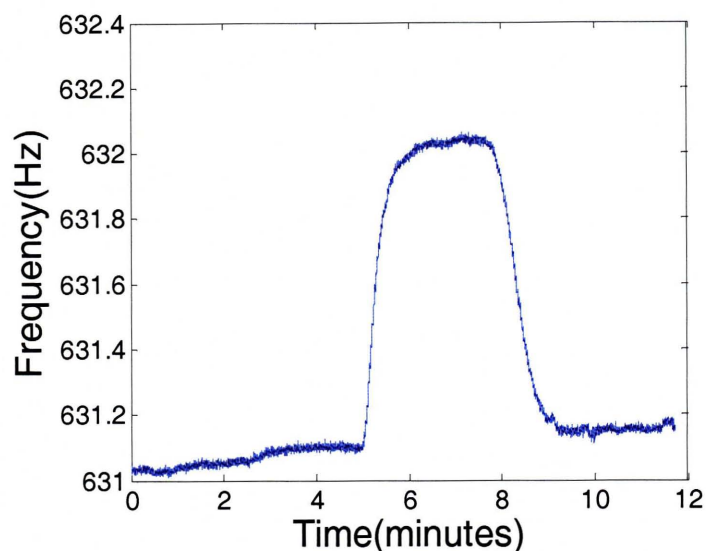


Figure 4. Peak response to the mobile phase as input. Peak height was reproducible irrespective of the concentration of the sample that was injected earlier, showing it is not carryover from the previous injection.

To determine the SMR detection limit, the baseline signal was acquired over a 90 second period with a 10 Hz sampling rate as the water eluted from a gel filtration column was driven through the bypass channel at a flow rate of 65 $\mu\text{L}/\text{min}$. The three standard deviation (3σ) of the resulting signal was found to be 9.6 mHz. The concentration sensitivity of the SMR was on the order of 0.1 $\text{g}/(\text{mL mHz})$ but differed slightly depending on the particular sample. That is, the detection limit resulting from sensitivities measured for glycine and glucose was approximately 2.5 g/mL , and for 8k PEG and BSA was approximately 5.5 g/mL . As shown in table 1, these values lead to the molar detection limit of 0.085 μM for BSA, 0.66 μM for 8 kDa PEG, 13.5 μM for glucose, and 31.6 μM for glycine.

Polyethylene glycol 8k	0.66 μM
Glucose	13.5 μM
Glycine	31.6 μM
Bovine Serum Albumin (BSA)	0.085 μM (0.97 nM in UV-Vis)

Considering the detection limit of 0.97 nM for BSA obtained by absorbance at 220 nm, UV-Visible absorbance is nearly 100-fold more sensitive than the SMR for samples with high extinction coefficients and detectors with sufficiently long optical path lengths. However, the SMR is more sensitive than RID. As shown in Table 2, in the case of weakly UV absorbing samples such as glycine, the SMR can resolve a concentration of ~2.5 g/mL in a 10 pL volume, whereas the commercial RID [10] resolves ~50 g/mL in a 8 μL volume.

Table 2. Typical Properties of the SMR and Other Common HPLC Detectors				
	ELSD [a]	UV-Visible [b]	RID [c]	SMR
Analyte response	Mass /volatility	Optical absorbance	Refractive Index	Mass
LOD for glycine [28]	5 μg/ml	2 μg/ml	50 μg/ml	2.5 μg/ml
Linear range	10 ¹ -10 ³	10 ⁴ -10 ⁵	10 ⁵	10 ⁶
Universal	Semi	No	Yes	Yes
a Sedex 55, Sedere (Vitry-sur-Seine, France)				
b L-2400, Merck-Hitachi(Merck, Darmstadt, Germany).				
c SpectraSYSTEM RI-150, Thermo Separation Product (Les Ulis, France).				

4.2 Dynamic range

An important aspect of detection by fluid density using the SMR is the wide dynamic range offered by the method. While the frequency noise of 3.2 mHz (10 Hz bandwidth) dictates the limit of detection for low concentrations, frequency changes as large as 10 kHz can be reliably measured. For example, a frequency shift of 10800 Hz results upon priming an air-filled cantilever with pure water. The dynamic range of the measurement therefore exceeds six orders of magnitude, with a maximum systematic deviation from linearity of 7.5%.

The deviation from the linear response comes from the non-linear relationship between resonant frequency and mass. The resonant frequency of the resonator is

$$f(m) = \frac{1}{2\pi} \sqrt{\frac{k}{m}} \quad (4)$$

(k: spring constant, m: the mass of the resonator)

Upon the added mass Δm , the Taylor expansion of the frequency to second order gives

$$f(m + \delta m) = \frac{1}{2\pi} \sqrt{\frac{k}{m + \delta m}} \approx f(m) - \frac{\sqrt{k}}{4\pi} m^{-\frac{3}{2}} (\delta m) + \frac{3\sqrt{k}}{16\pi} m^{-\frac{5}{2}} (\delta m)^2 \quad (5)$$

The relative frequency change is given by

$$\frac{f(m + \delta m) - f(m)}{f(m)} \approx -\frac{(\delta m)}{2m} + \frac{3(\delta m)^2}{8m^2} \quad (6)$$

Since the first term of the right hand side is linear, the frequency shift is linear to the added mass δm if

$\frac{(\delta m)}{2m} \gg \frac{3(\delta m)^2}{8m^2}$. Hence, if $\delta m \ll m$ the response can be assumed as linear.

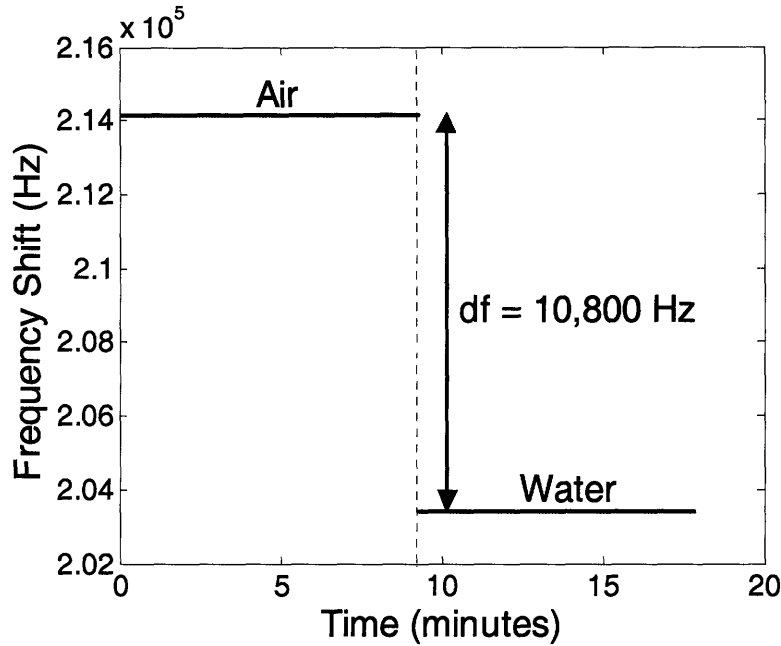


Figure 5. Frequency response to air and water respectively. To avoid the response due to the pressure difference, there was no net flow during the measurement. Response to air to water transition was removed for simplicity. Mean value of the air frequency is 214200 Hz and the mean value of water frequency is 203400 Hz, which gives the frequency shift of 10800 Hz.

The resonator mass m is reported as 100 ng and the volume is 10 pL. Upon the sample change from air to water, the mass change is $\delta m = \Delta V \rho = 10$ ng. Comparing the first and the second term of equation (6), it

shows there is 7.5 % deviation from the linear response when the sample changes from air to water. For the reported density sensitivity of 10470 Hz/(g·cm⁻³), water ($\rho = 1 \text{ g cm}^{-3}$) and air ($\rho = 0.0012 \text{ g cm}^{-3}$), the transition will give a ~10 kHz frequency shift which is confirmed by our measurement. In figure 5, the transition gives 10800 Hz frequency shift, showing 3.3 % deviation from the linear response.

4.3 Chromatogram

To demonstrate that SMR detection can be used for real-time eluate monitoring, a chromatogram was acquired from a gel filtration chromatography (GFC) separation. A 3 μL sample of a PEG mixture containing various molecular weights (1 kDa, 4 kDa, 8 kDa, 20 kDa, and 31 kDa; 5 mg/ml each) was injected at a flow rate of 65 $\mu\text{L}/\text{min}$ in a mobile phase of purified water. To validate the SMR response, a chromatogram was also acquired by measuring the UV-Visible absorbance of the eluate at a wavelength of 196 nm (4 nm bandwidth and slit width). As shown in figure 6, the retention time, peak width, and resolution are well matched in both chromatograms.

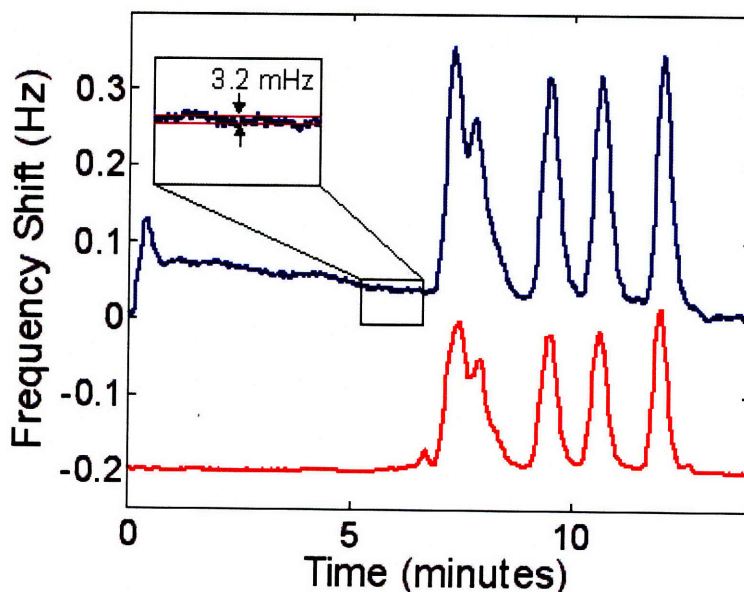


Figure 6. Chromatograms resulting from the HPLC separation and SMR (top) or UV-Visible (bottom) detection of a five-component mixture of polyethylene glycol (31 kDa, 20 kDa, 8 kDa, 4 kDa, and 1 kDa in order eluted). In the inset, the baseline noise of the SMR for 90 seconds shows the standard deviation of 3.2 mHz. The UV-Visible chromatogram was offset vertically from the SMR chromatogram for clarity (1 Hz equal to 250 mAU in UV-Visible.).

The short-term instability of the SMR baseline was primarily due to variations in pressure. For

example, the peak at $t \sim 0.3$ min was due to a pressure increase induced by switching the injection valve from the loading to running position. Even though large pressure changes during elution are not expected, the viscosity differences within the eluted sample effectively alter the pressure and induce signal artifacts. In addition, the active flow rate control of the HPLC pump can cause periodic pressure changes which can be observed from the SMR signal as well. However, these variations can be compensated for off-line by calibrating the frequency-pressure relationship. Alternatively, using another elution mechanism such as electrokinetic separation could avoid this problem. The long term drift (approximately 100 mHz over 10 minutes) was primarily due to drift in ambient temperature. We anticipate that this drift could be eliminated by either using temperature control or making a differential measurement with an adjacent SMR sensor [21].

4.4 Gradient elution

Gradient elution is very useful in eluting complex mixtures because of the variable interactivity of the mobile phase. However, universal detectors such as RID are usually incompatible with gradient elution due to the lack of specificity to sample. Since SMR might also be incompatible with conventional gradient elution, we verified the feasibility of the use of the SMR in gradient elution by modifying the eluting method.

The idea is to conduct the identical gradient elution twice, with or without the sample injection. By subtracting the signal obtained without the sample injection from the signal obtained with the sample injection, we can remove the background signal induced by the change of the mobile phase. To prove this concept, we first conducted gradient elution of BSA with the mobile phase that changes from pure water to pure acetonitrile in 30 minutes and measured the response by UV detector at the wavelength of 192nm, where the response is almost universal.

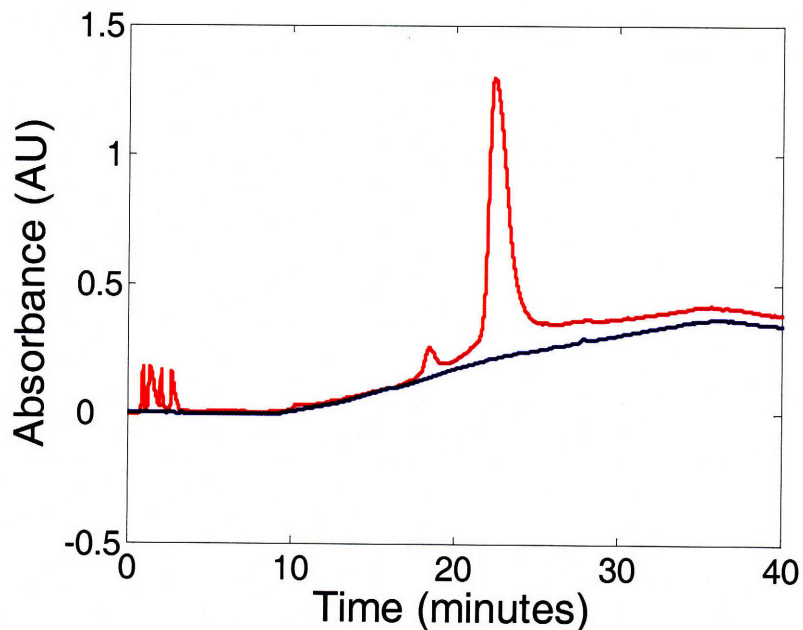


Figure 7. Chromatograms resulting from the two serial runs of the identical gradient elution with (top) or without (bottom) the sample injection. 10 μL of 0.2 % BSA was injected to the reverse phase column with the mobile phase flow rate of 15 $\mu\text{L}/\text{min}$ and detected by UV detector at the wavelength of 192 nm. The mobile phase was changed from pure water to 100 % acetonitrile in 30 minutes. The large peak at 22.5 minutes shows most of BSA is eluted in 40 % acetonitrile. The first sets of small peaks are unretained peaks and the small peak close to the large peak is attributed to the impurity of BSA sample.

In figure 7, the peak of BSA is superimposed on the baseline signal, which was attributed to the mobile phase change. The baseline signal can be further eliminated from the chromatogram as shown in figure 8 by subtracting the signal of the blank run from the signal of the run with the sample injection to compensate for any reproducible ghost peak. To validate the compensated signal, we compared it to the chromatogram of the same run obtained at the wavelength of 220 nm, which is specific to BSA and conventionally used to detect BSA in reverse phase chromatography. In general, both chromatograms show the same response proving the validity of the compensated chromatogram. The smaller tail height of the compensated signal is considered a result of normalization when the large peak of compensated signal (~ 1.1 AU) exceeds the dynamic range of UV detector.

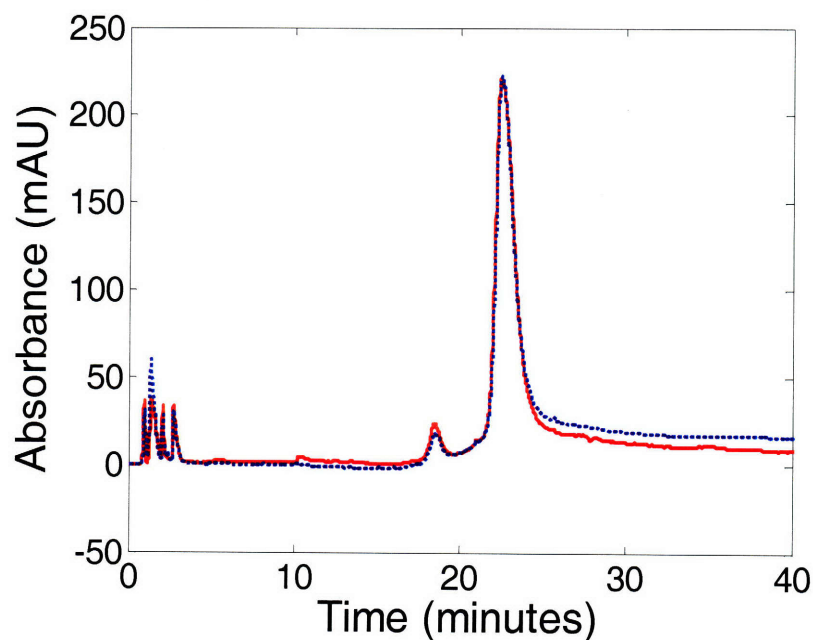


Figure 8. Chromatogram resulting from the elimination of the baseline signal of figure 7 (solid line). The same gradient elution was detected by UV detector at the wavelength of 220 nm, which is specific only to BSA (dotted line). In both case, they show one small peak and one large peak with the long flat tail. The compensated signal (top) is normalized to the other signal to help comparing both chromatograms.

We conducted the identical gradient elution with the SMR as a detector. However, since the baseline signal was very large compared to the signal of 0.2 % BSA, it was hard to identify the peaks without the compensation of the baseline signal. That is, 0.2 % BSA gives ~ 1.5 Hz frequency response while the change of mobile phase from water to 100 % acetonitrile gives ~ 2300 Hz frequency response (data not shown). Figure 9 shows the compensated signal obtained by subtracting the baseline signal from the signal with the sample injection.

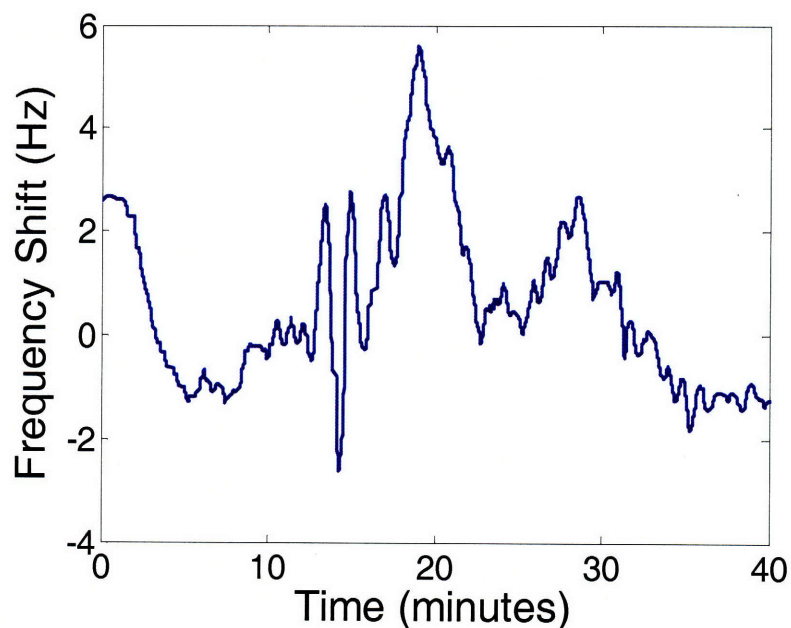


Figure 9. Chromatogram of the SMR resulting from the elimination of the baseline signal after two identical gradient elutions with or without the sample injection. 10 μL of 0.2 % BSA was injected to the reverse phase column with the mobile phase flow rate of 15 $\mu\text{L}/\text{min}$. The mobile phase was changed from pure water to 100 % acetonitrile in 30 minutes. Baseline drifts over 2 Hz.

In figure 9, it is hard to define the estimated BSA peak of ~ 1.5 Hz due to the baseline drift over 2 Hz. Since the SMR response is not specific to BSA, any difference in chromatographic condition between two gradient elutions can contribute to the baseline drift. For example, the ambient temperature change can serve as a main source of the baseline drift because the frequency shifts by ~ 3.3 Hz/ $^{\circ}\text{C}$. The change in mixing and pumping conditions can also induce the baseline drift. Even though it is assumed that the HPLC system can maintain the same mobile phase composition and flow rate over the two identical runs, it can never happen in practice. Since the SMR is very sensitive to the ratio of acetonitrile in mobile phase, even the small difference of the mobile phase composition at the given time will induce the large baseline drift. In addition, the pressure change is not negligible because the SMR is sensitive to the pressure as well.

To improve this experiment, we can connect the adjacent cantilever in series to measure the signal with or without the sample injection in one gradient elution. Temperature control during the elution will also help stabilizing the baseline drift since we observed the baseline was stabilized below 0.1 Hz over the one entire run (~ 40 min) when we used a water bath temperature controller with 0.01°C stability. (ThermoNesLab RTE7, Thermo Fisher Scientific, Inc.) (data not shown) In conclusion, while it is not straightforward for the

SMR to measure the gradient elution signal, there remain more ideas to be tested to prove the feasibility of SMR in use of gradient elution.

4.5 Peak dispersion

The finite nature of the detector sensor volume can cause peak dispersion and contribute to the peak variance by two processes [22]. Firstly there will be a dispersion resulting from convection of the Newtonian flow through the cell. Since most sensor volumes are cylindrical in shape and relatively short in length, having a small length-to-diameter ratio, convection serves as a main source of dispersion. Secondly, there will be a peak spreading resulting from the finite volume of the sensor. If the sensor has a significant volume, the concentration measured will not be that entering the detector cell but the average concentration throughout the cell, resulting in the loss of resolution. In the extreme case two peaks could coexist in the sensor at one time and only a single peak will be detected. This problem can be particularly severe in microscale separation, where the sample volume is very small.

The SMR is advantageous in that the cell has relatively large length-to-diameter ratio (200 μm in length, 3 μm by 8 μm rectangle in cross section) and very small volume (10 pL). In this case, dispersion due to convection and peak spreading in the sensor can be minimized, which becomes especially useful when the sensor is integrated to μ -TAS, where the sample volume is very small.

To demonstrate the different response of the SMR and the UV detector to the small sample injection, we simulated the 2D diffusion of Newtonian flow in a 2 D conduit in Poiseuille flow profile. We focused only on the dispersion inside the detector cell, ignoring any other source of dispersion. That is, it was assumed that the sample is injected directly to the detection cell without passing through the separation column or tubing. The diffusion equation in combination with convection is

$$\frac{\partial C}{\partial t} + \nabla \cdot (uC) = D\nabla^2 C \quad (7)$$

(C: concentration, t: time, u: linear flow velocity, D: diffusion coefficient)

Using Matlab, this equation was solved and applied to Poiseuille flow profile (Appendix A). Figure 10 is the graphical representation of the solution, showing the diffusion and the convection of the peak. It shows convection dominates diffusion when the diffusion coefficient is fairly large and the length of the tubing between the separation column and the detector is short. Convection induces the loss of the signal when the peak area inside the detector cell is averaged to the concentration signal at the given time.

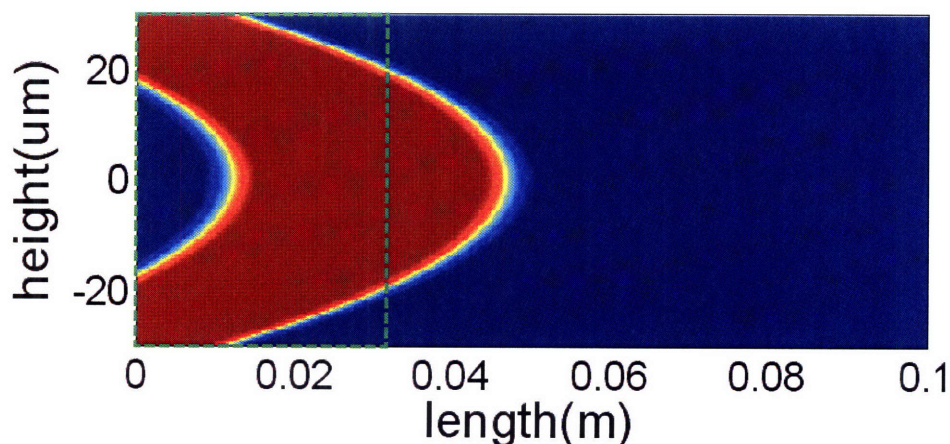


Figure 10. Concentration profile of 100 μL sample band 1 second after it enters to the UV detector cell, whose area is defined by the green dotted box. The diameter and the length of the UV detector are assumed as 60 μm and 3 cm respectively, resulting in the volume of 80 nL. Diffusion coefficient of the band is $10^{-6} \text{ m}^2/\text{s}$ and the flow rate is 3 $\mu\text{L}/\text{min}$. Concentration is maximum in red and minimum in blue.

As mentioned before, signal averaging induced by convection decreases when the cell has relatively large length-to-diameter ratio and very small volume. In figure 11, not only is the peak larger in the SMR than in the UV detector, but also the retention time is shorter in the SMR. Considering the retention time is the determining factor of the chemical or physical property of the sample, such as affinity or size, the delay in the retention time is even more crucial than the peak shortening. In addition, the UV detector response shows severe peak broadening, which induces the loss of resolution.

Even though the experiment of the above simulation was straightforward, our analytical scale HPLC system had several limitations dealing with the microscale sample due to the high minimum flow rate and the need of several centimeters of connection from the separation column to the detector. In addition, the bypass channel in the SMR designed to accommodate high flow rate also serves as a source of dispersion when dealing with the small amount of sample. However, given the simulation results and the unique scaling property of the SMR we believe the SMR can be integrated to $\mu\text{-TAS}$ to minimize the peak broadening and delay in the retention time.

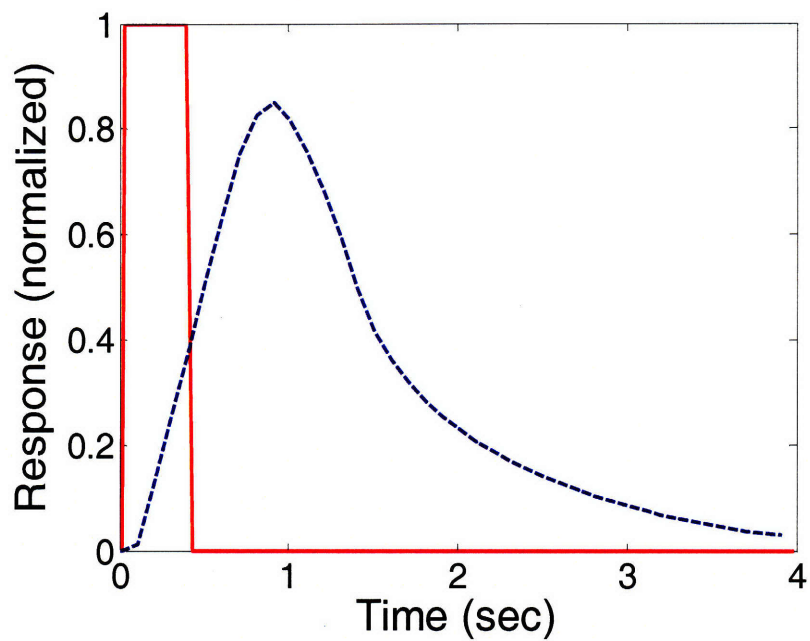


Figure 11. Simulated response of the SMR (solid line) and the UV detector (dotted line) to 100 μL sample injection in 3 $\mu\text{L}/\text{min}$ flow rate. Response is normalized to maximum 1. The diameter and the length of the UV detector are assumed as 60 μm and 3 cm respectively, resulting in the volume of 80 nL. The diameter and the length of the SMR are assumed as 8 μm and 200 μm respectively, resulting in the volume of 10 pL.

5. Conclusion

We have demonstrated that the SMR can be used for real-time universal detection. When compared to a state-of-art commercial RID system [10], the SMR achieves a more than 10-fold improvement in detection limit (as determined with glycine) for an analysis volume that is 10^5 -fold smaller. Since the SMR is a batch fabricated microfluidic device, it can be readily integrated within micro total analysis systems (μ TAS) without compromising overall performance [26]. The device used throughout this work is already compatible with the volumes and flow rates typically available in microfluidics, and with appropriate integration, similar results should be attainable in the context of detection in μ TAS. Moreover, the detection limit of the SMR as determined by the thermomechanical noise is approximately 4 ng/cm^3 and we anticipate that optimization of the frequency detection circuitry will ultimately allow us to approach this limit.

We envision that the SMR's ability to detect the binding of specific molecules to its interior surface could enable immunoaffinity CE (IACE) applications [27]. We recently showed that, using a monolayer coverage (2 pmol cm^{-2}) of active antibodies with a dissociation constant of 1 nM , the SMR can detect the binding of a 30 kDa analyte with a detection limit on the order of 1 pM [21]. For multi-analyte detection, arrays of SMRs could be functionalized with different capture molecules.

6. Appendix

A. Matlab code.

```
clear all;
close all;

% change SMR cell shape, diffusion coefficient, slip length to fit the curve to experimental
data

D=10^-6;           % diffusion coeff [m^2/s]
fr_volu=3;         % volumetric flow rate (ul/min)
inj_volu=0.1;      % injection volume (ul)
ly=60*10^-6;       % capillary id [m] (60um)
lx=0;              % capillary length [m] (1m)
im_l=.1;           % imaginary capillary length [m]
det_kind=1;        % uv: 1 smr: 2

B=5*10^-6;         % slip length [m] (1um)
fr_vol=fr_volu*10^-9/60; % [m^3/sec]
inj_vol=inj_volu*10^-9; % [m^3]
nx=500;ny=200;     % array dimension
umax=2*4*fr_vol/pi/ly^2; % max velocity [m/sec]
lp=inj_vol/pi/(ly/2)^2; % plug length [m]
MM=100;            % conc plot size

x=linspace(0,im_l, nx);
y=linspace(-ly/2, ly/2, ny);
[X,Y]=meshgrid(x,y);

z=zeros(size(X)); % initialize conc data
c0=1;             % initial conc
t=1;              % elapsed time
```

```

u=zeros(size(y));    % initialize velocity data

% flow profile
u=umax*((1-(y/(ly/2)).^2)+2*B/(ly/2));

% diffusion
tt=zeros(MM,1);
cconc=zeros(MM,1);
i=1;
tt(i)=0;cconc(i)=0;
for t=0.01:.1:2
    % cell concentration
    i=i+1;
    if det_kind == 1
        cell_d=80*10^-12/pi/(ly/2)^2;    % cell_length [m]
        C=z(:,min(find(x>lx)):min(find(x>lx+cell_d)-1));
        ll=ly;
    elseif det_kind == 2
        cell_d=1.1*10^-14/pi/(ly/2)^2;    % cell_length [m]
        C=z(round(ny-ny/30):ny,min(find(x>lx)):min(find(x>lx+cell_d)-1));
        ll=ly/30;
    end
    ssum=sum(sum(C));
    size_mat=size(C);
    sat=size_mat(1)*size_mat(2);
    tt(i)=t;
    cconc(i)=ssum/sat;
    figure;
    subplot(2,1,2);
    plot(tt(1:i), cconc(1:i), '-');
    axis([0, max(tt), 0,1]);
    xlabel('time(sec)');
    ylabel('Conc(Normalized)');
    grid on;

```

```

hold on;

% 2D conc profile
for r=1:ny
    z(r,:)=c0/2*(erf((x+lp-u(r)*t)/sqrt(4*D*t))-erf((x-u(r)*t)/sqrt(4*D*t)));
end

subplot(2,1,1);
pcolor(X,Y*10^6,z);%hold on;
title('Convective and axial diffusion in straight channel');
xlabel('length(m)');ylabel('height(m)');
rectangle('Position', [lx, -ly/2*10^6, cell_d, ll*10^6]);shading interp;
colormap pink;

end

```

7. References

1. E.S. Yeung (Editor), *Detectors for Liquid Chromatography*, Chemical Analysis 89.; Wiley: New York, 1986.
2. Weston, A.; Brown, P. R. *HPLC and CE: Principles and Practice*, 1st ed.; Academic Press: London, 1997.
3. Moreau, R. A.; Powell, M. J.; Hicks, K. B. *J. Agric. Food Chem.* **1996**, *44*, 2149-2154.
4. Wei, Y.; Ding, M. Y. *J. Chromatogr., A* **2000**, *904*, 113-117.
5. Asmus, P. A.; Landis, J. B. *J. Chromatogr.* **1984**, *316*, 461-472.
6. Strege, M. A.; Stevenson, S.; Lawrence, S. M. *Anal. Chem.* **2000**, *72*, 4629-4633.
7. Scott, R. P. W. *In Analytical Instrumentation Handbook*; Ewing, G. W. Ed.; Marcel Dekker: New York, 1997; pp 1123-1203.
8. Ravindranath, B. *Principles and Practice of Chromatography*; Halsted Press: New York, 1989.
9. Wang, Z.; Bornhop, D. J. *Anal. Chem.* **2005**, *77*, 7872-7877.
10. Thermo Electron Corporation. *Product Specifications*. **2003**.
11. Trathnigg, B. and Jorde, C. *J. Chromatogr.*, **1987**, *385*, 17-23.
12. Yang, F. *J. High Resolut. Chromatogr. Chromatogr. Commun.*, **1981**, *4*, 83.
13. Markov, D. A.; Swinney, K.; Bornhop, D. J. *J. Am. Chem. Soc.* **2004**, *126*, 16659-16664.
14. Swinney, K.; Pennington, J.; Bornhop, D. J. *Microchem. J.* **1999**, *62*, 154-163.
15. Bruno, A. E.; Paulus, A.; Bornhop, D. J. *J. Appl. Spectrosc.* **1991**, *45*, 462-467.
16. Bruno, A. E.; Krattiger, B.; Maystre, F.; Widmer, H. M. *Anal. Chem.* **1991**, *63*, 2689-2697.
17. Wang, Z.; Bornhop, D. J. *Anal. Chem.* **2005**, *77*, 7872-7877.
18. Bornhop D. J.; Latham J. C.; Kussrow A; Markov D. A.; Jones R. D.; Sorensen H. S. *Science*. **2007**, *317*, 1732-1736.
19. Corman T.; Enoksson P.; Noren K.; Stemme G. *Meas. Sci. Technol.* **2000**, *11*, 205-211.
20. Sparks D.; Smith R.; Straayer M.; Cripe J.; Schneider R.; Chimbayo A.; Anasari S.; Najafi N. *Lab. Chip.* **2003**, *3*, 19-21.
21. Burg, T. P.; Godin, M.; Knudsen, S. M.; Shen, W.; Carlson, G.; Foster, J. S.; Babcock, K.; Manalis, S. R. *Nature* **2007**, *446*, 1066-1069.
22. Scott, R. P. W. *Liquid Chromatography Detectors*. 2nd ed.; Elsevier Scientific: Amsterdam, **1986**.
23. Scott, R. P. W. *Liquid Chromatography*. <http://www.library4science.com/>, **2003**.
24. Zhu, Hongying.; White, I. M.; Suter, J. D.; Zourob, Mohammed; Fan, Xudong. *Anal. Chem.* **2007**, *79*, 930-937.

25. Lv, Yi.; Zhang, Sichun.; Liu, Guohong.; Huang, Minwen.; Zhang, Xinrong. *Anal. Chem.* **2005**, *77*, 1518-1525.
26. Burg, T. P.; Manalis, S.R. *J. Microelectromech. Syst.* **2006**, *15*, 1466–1476.
27. Guzman, N. A. *Anal. Bioanal. Chem.* **2004**, *378*, 37-39.
28. Petritis K.; Elfakir C.; Dreux M. *J. Chromatogr. A* **2002**, *961* 9-21.